 doi:10.20944/preprints202109.0019.v1

Article

New Edge Crush Test Configuration Enhanced with Full-Field Strain Measurements

Tomasz Garbowski [1], Anna Knitter-Piątkowska [2,*] and Aleksander Marek [3]

[1] Department of Biosystems Engineering, Poznan University of Life Sciences, Wojska Polskiego 50, 60-627 Poznań, Poland; tomasz.garbowski@up.poznan.pl
[2] Institute of Structural Analysis, Poznan University of Technology, Piotrowo 5, 60-965 Poznań, Poland
[3] Faculty of Engineering and Physical Sciences, University of Southampton, Highfield SO171BJ, UK; a.marek@soton.ac.uk
* Correspondence: anna.knitter-piatkowska@put.poznan.pl

Abstract: The standard edge crush test (ECT) allows to determine the crushing strength of the corrugated cardboard. Unfortunately, this test cannot be used to estimate the compressive stiffness, which is an equally important parameter. It is because, any attempt to determine this parameter using current lab equipment quickly ends in a fiasco. The biggest obstacle is obtaining a reliable measurement of displacements and strains in the corrugated cardboard sample. In this paper, we present a method that not only allows to reliably identify the stiffness in the loaded direction of orthotropy in the corrugated board sample, but also the full orthotropic material stiffness matrix. The proposed method uses two samples: (a) traditional, cut crosswise to the wave direction of the corrugated core, and (b) cut at an angle of 45 degrees. Additionally, in both cases, an optical system with digital image correlation (DIC) is used to measure the displacements and strains on the outer surface of samples. The use of a non-contact measuring system allows to avoid using the measurement of displacements from the crosshead, which is burdened with a large error. Apart from the new experimental configuration, the article also proposes a simple algorithm to quickly characterize all sought stiffness parameters. The obtained results are finally compared with the results obtained in the homogenization procedure of the cross-section of the corrugated board. The results were consistent in both cases.

Keywords: corrugated cardboard; edge crush test; orthotropic elasticity; digital image correlation, tensile stiffness, compressive stiffness, sandwich panel

1. Introduction

The increasing consumer demands and absorptive power of the merchant market in today's world, resulting in the need of packing, storage and secure shipping of more and more various goods, as well as the growing ecological awareness have led to the increasing interest of manufacturers in cardboard packaging. This fact, in turn, has triggered an inevitable, continuous and intensive development of numerous corrugated cardboard testing techniques over the last decades.

Assessing the load-bearing capacity of the corrugated cardboard products is crucial for their proper designing, production and final usage or even re-use processes. It is important to emphasize here that corrugated cardboard comprises a few layers thus can be called a sandwich structure. Its mechanical properties are directly related to two characteristic in-plane directions of orthotropy, i.e., machine direction (MD) that is perpendicular to the main axis of the fluting and parallel to the paperboard fiber alignment and cross direction (CD) which is parallel to the fluting.

Numerous approaches for sandwich elements strength determination, including the corrugated cardboard, can be found in the literature. Analytical methods, starting already

in the fifties of the twentieth century, were presented, i.a., in [1–5], whereas numerical methods can be found in [6–11] and analytical-numerical techniques in [12–16]. Analytical calculation of the edge crush resistance of cellular paperboard, both in MD and CD while basing on the paperboard's geometric parameters and the mechanical properties of materials used for its production, was discussed by Kmita-Fudalej et al. [17]. Park et al. [18] investigated the edgewise compression behavior of corrugated paperboard while applying finite element method (FEM) as well as experimental analysis, i.e., load vs. displacement plot, edge crush test (ECT) and failure mechanism. In recent years, methods of artificial intelligence, including artificial neural networks, have become widespread to predict the strength of composite materials, e.g., sandwich structures as presented by Wong et al. [19].

While executing numerical simulations in examining the corrugated cardboard, the comprehensive knowledge of all layers' material properties is necessary. Due to the anisotropy of the paper-based materials this is a demanding task. In such a case a good solution is to implement a method called homogenization. This approach efficiently allows to simplify the multi-layer models into single-layered, described by the effective properties of the composite [9,10,20]. Application of this technique benefits in significant savings in computation time while maintaining the accuracy of the results. Hohe [21] presented the strain energy approach applicable to sandwich panels for homogenization and proposed an equivalence of a representative element of the heterogeneous and homogenized elements for this purpose.

Another option, in addition to analytical or numerical analysis, for estimation of corrugated board strength is to carry out measurements from the experiment. Physical testing is very common in the paper industry, and a number of typical tests have been developed to unify the process of characterization of corrugated cardboard mechanical properties. The aforementioned ECT is used to evaluate the compressive strength, the load during this examination is applied perpendicularly to the axis of the flutes. In the bending test (BNT), four-point bending is executed, two supports are at the bottom of the cardboard whereas two equal forces acts on the sample from the opposite side. The shear stiffness test (SST) involves twisting of the cardboard cross-section by applying a pair of forces to opposite corners while the other two remain supported. In torsional stiffness test (TST) the cardboard sample is twisted in both directions. The box compressive test (BCT) is conducted to examine the load bearing capacity of the whole cardboard box [12–14,22]. The bursting and humidity tests should also be mentioned here.

Since ECT is standardized, four different methods have been described, i.e., edge-clamping method [23], neck-down method [24], rectangular test specimen method [24–26] and edge-reinforced method [27,28]. One of the major characteristics which differs these tests is the shape of the specimens. To assemble the measurements from the outer surfaces of the sample during the examination a video extensometry can be employed. Such a procedure is based on the measurement of the relative distances between pairs of points traced across images captured at different load values [15]. This is a comparable yet simpler method than digital image correlation (DIC) which, as full-field non-contact optical measurement method, is gaining more popularity in the field of experimental mechanics since it ensures very high accuracy of data acquisition. Hägglund et al. applied DIC while examining thickness changes during the ECT in the damaged and undamaged panels made of corrugated paperboard [29]. Implementation of DIC for investigation of strain and stress fields of paperboard panels subjected to BCT and analysis of their post buckling behavior was discussed by Viguié et al. in [30–32]. A distortional hardening plasticity model for paperboard was presented by Borgqvist et al. [33] who introduced a yield surface characterized by multiple hardening variables attained from simple uniaxial tests. The comparison between the results acquired from the model and experimental, received while using DIC, was demonstrated as well. Combined compression and bending tests of paperboards and laminates for liquid containers while applying DIC were executed by Cocchetti et al. [34,35] who identified material parameters of anisotropic elastic-plastic

 doi:10.20944/preprints202109.0019.v1

material models of foils. For this purpose inverse analysis was employed while processing the results received from both the experiment and numerical FEM simulations. DIC and the virtual fields method (VFM) for recognition of general anisotropy parameters of a filter paper and a paperboard have been discussed by Considine [36]. Åslund et al. applied the detailed FEM for investigation of the corrugated sandwich panels failure mechanism while performing the ECT and compared the results with the measurements obtained with the use of DIC [37]. Zappa et al. studied the inflation of the paperboard composites which are used in the packaging of beverages while applying DIC [38]. Paperboard boxes with ventilation holes subjected to a compression load were investigated involving DIC by Fadiji et al [39].

It should be pointed out that in a large part of the above-mentioned studies 3-ply corrugated cardboards specimens were tested. In this research a double-wall corrugated cardboard, i.e., 5-ply samples are examined. While performing ECT an optical system with digital image correlation (DIC) is used to measure the displacements on the outer surface of the specimen. The proposed method uses two types of samples, i.e., traditional, cut crosswise to the direction of the wave direction of the corrugated core, and, what is a novel procedure, cut at an angle of 45 degrees. Such an approach not only allows to reliably identify the stiffness in one direction of orthotropy, but the full material stiffness matrix, i.e., 4 independent parameters. Obtained results were verified by the results acquired in the homogenization procedure of the cross-section of the corrugated board. As proven, in both cases, the results were very consistent.

2. Materials and Methods

2.1. Corrugated Cardboard

In this study, a 5-layer corrugated cardboard marked as EB-650 was used. The top liner is made of white, coated, recycled cardboard TLWC with a grammage of 140 g/m^2. The cross-section has two corrugated layers: (a) low flute (E wave) and (b) high flute (B wave). Both wavy layers and the flat layer between them, forming the mid liner, are made of lightweight WB cardboard, also recycled, with a grammage of 100 g/m^2. As a bottom liner again the white recycled test liner with a grammage of 120 g/m^2 was used. The geometry of the cross-section of the corrugated board and the arrangement of the individual layers are shown in Figure 1, where 5 samples are placed one on top of the other.

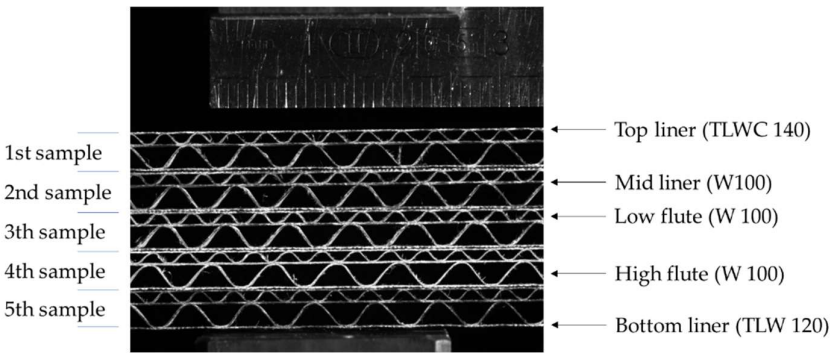

Figure 1. Visualization of 5 samples (stacked on top of each other) of the analyzed corrugated cardboard.

Table 1 presents the geometrical parameters of both wavy layers (flutes). Second and third column of Table 1 shows the wave period (pitch) and the wave amplitude (height), respectively. Take-up ratio, which defines the ratio of the length of the non-fluted corrugated medium to the length of the fluted web are given in the last column of Table 1.

 doi:10.20944/preprints202109.0019.v1

Table 1. The geometrical features of both corrugated layers of EB-650.

Wave (Flute)	Pitch (mm)	Height (mm)	Take-up Ratio (–)
E	3.50	1.18	1.242
B	6.48	2.5	1.315

Paperboard, which is a main component of corrugated board is made of cellulose fibers. Their orientation is not random, but rather results from the production process, which causes that the vast majority of the fibers are arranged along the web, called machine direction (MD). The second direction, perpendicular to the MD is called cross direction (CD). Paperboard is both stronger and stiffer along the fibers direction.

In general, materials whose mechanical properties depend on the fibers orientation are called orthotropic materials. As a component of corrugated cardboard, paper also makes it an orthotropic material. The orientation of the fibers, shown in Figure 2, makes the corrugated board stronger along the direction of the wave. Thus, the corrugated layers compensate (through the take-up factor) for the weaker mechanical properties of the board in CD.

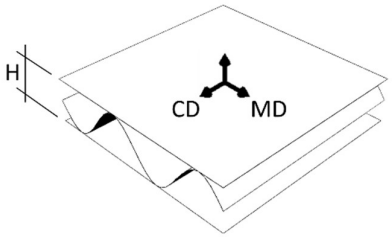

Figure 2. The material orientation in the corrugated board.

Table 2 presents the material properties of the individual layers of the corrugated board. The compressive strength in CD, SCT_{CD}, is measured using the short-span compression test according to DIN EN ISO 3037 [26]. The compressive strength of the combined corrugated board in CD, ECT_{CD}, specified by the producer–Aquila Września–is 7.6 kN/m (±10%), while the overall thickness of the EB-650, H is 4.3 mm (±0.2 mm).

Table 2. Mechanical properties of individual layers of 5EB650C3.

Layer Name	Thickness (µm)	E_{MD} (kN/m)	E_{CD} (kN/m)	SCT_{CD} (kN/m)
TLWC 140	180	725	323	2.32
W 100	160	886	328	1.76
TLW 120	170	907	313	1.81

2.2. The Edge Crush Test

The Edge Crush Test (ECT) is a typical test to determine the compressive strength of corrugated board. The test is performed according to FEFCO DIN EN ISO 3037 [25,26], where a 100 mm long and 25 mm high specimen (see Figures 3a and 3b) is loaded between two rigid plates along its height (see Figure 4a). In order to maintain the parallelism of the cut edges of the sample, it should be cut on a special device, e.g. FEMat CUT device [22] (see Figure 4b) where the samples are pneumatically cut with one-sided ground blades. All ECT tests were performed under controlled and standard air conditions, i.e. 23°C and 50% relative humidity.

As already mentioned above, the typical ECT is only used to determine the compressive strength of the corrugated board in CD. Here, the new ECT test setup was also used

Preprints (www.preprints.org) | NOT PEER-REVIEWED | Posted: 1 September 2021 doi:10.20944/preprints202109.0019.v1

to determine all elastic orthotropic properties of the in-plane tension / compression behavior of corrugated cardboard. For this purpose, beside traditional, also samples cut at an angle of 45 degrees to the wave direction were used (see Figures 3c and 3d). Since the measurement in standard testing machines is significantly affected by the clearance and susceptibility on the crosshead, non-contact optical techniques are required to reliably measure displacements (deformations or strains).

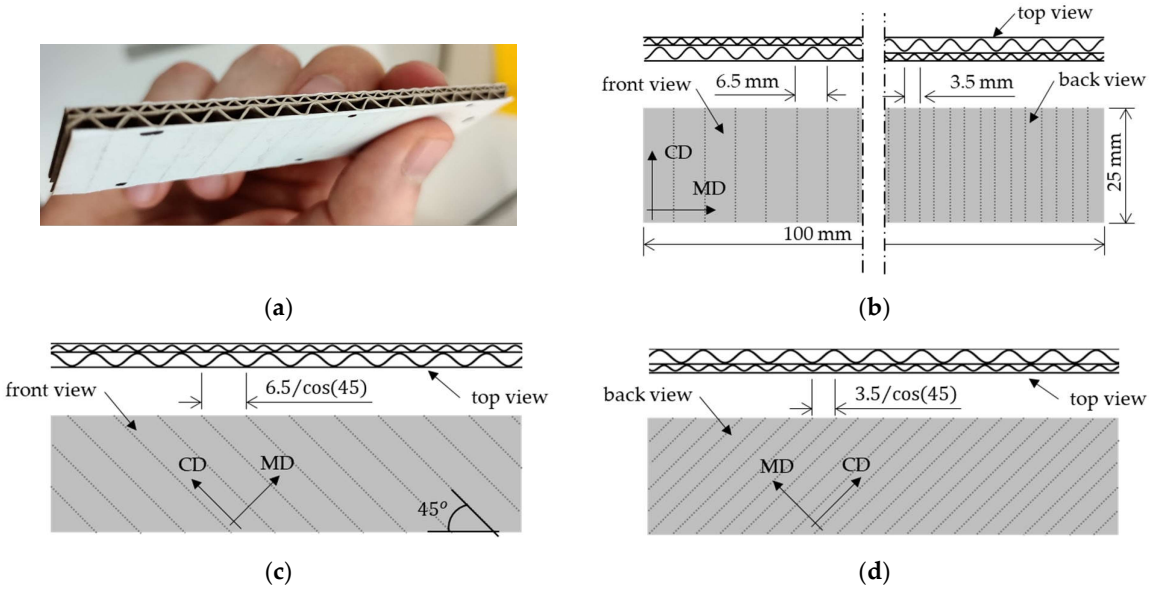

Figure 3. The sample for the standard and new edge crush test: (**a**) standard sample view; (**b**) standard ECT sample – front, back and top view; (**c**) new ECT sample – front and top view; (**d**) new ECT sample – back and top view

Additionally, measurement without direct contact does not affect the measurement itself. In contact measurements (e.g. traditional extensometers), noise is introduced into the measurement, which may distort the actual measured values.

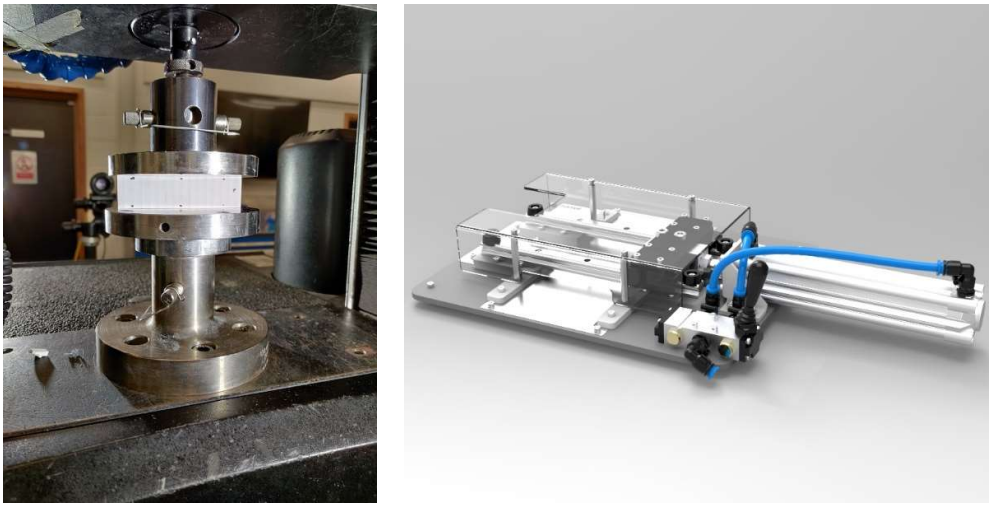

Figure 4. Edge crush test: (**a**) Universal Testing Machine (Instron 5569); (**b**) FEMAT lab device.

2.3. Optical Measurements of Sample Deformation

 doi:10.20944/preprints202109.0019.v1

In this study, as was already mentioned, the specimen was tested using optical displacement and strain measurements, i.e., virtual extensometry and Digital Image Correlation (DIC). Two cameras (the stereo DIC setup) were used to track the deformation on the front faces to account for the out-of-plane bending produced by the non-symmetrical section and single camera on the back faces meant to use only optical extensometry, see the test setup on Figure 5a. Each of the two faces of the specimen were printed with the speckle pattern for both optical methods, i.e., DIC and video extensometry. Here, three models of deformation measurements were used, namely:

- Crosshead from the machine;
- Stereo (2.5D) DIC on the front (see Figure 5b) + extensometry on the back;
- Extensometry on the front and back.

The specimen was sandwiched between two platens and aligned while using 3D printed L-brackets. Two 5 MPix cameras (Manta G504-b, Allied Vision, Stadtroda, Germany) were used to record grey scale images during the test, see Figure 5. The video extensometry was performed using MatchID DIC platform (v. 2020.2.0, MatchID, Ghent, Belgium). Cameras were calibrated while applying MatchID calibration plate (MatchID, Ghent, Belgium) to obtain the pixel to mm conversion rate of ~50 μm/pix. The specimen was manually preloaded with a very small load (15 N) to ensure that both edges of the specimen were touching the loading plates. Then the measured load cell and displacement were zeroed and the L-brackets supporting the sample were removed. The load and the crosshead displacement were synchronized with the cameras. The accuracy of the measurement was estimated while using a set of 25 static images (without any movement); standard deviation of the measured elongation was evaluated to be 4 μm, which can be considered the level of uncertainty. Optical displacements were averaged for each face and compared against the crosshead displacement.

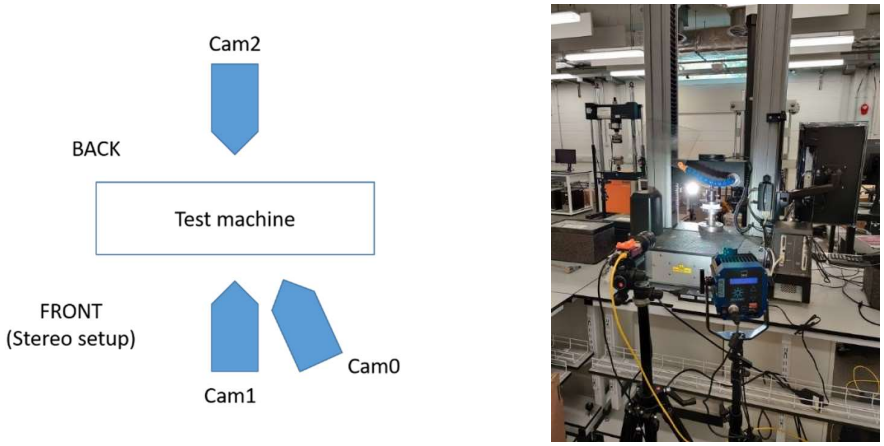

(**a**) (**b**)

Figure 5. Setup of the optical measurements: (**a**) configuration of cameras on the front and back face; (**b**) cameras recording the front face.

In total, 5 samples in CD and 5 in 45 deg direction were tested. Unfortunately, one of the sample in CD was not recorded properly on the PC and was removed from the statistics. The loading rate was set to 5 mm/min (which is different from the standard rate 12.5 mm/min) because samples failed to fast for cameras to get enough data.

The following stereo DIC procedures, with camera 'Cam1' as the main one, were utilized in this research:

- Perform DIC on the sample's face while using images from Cam1 and Cam0; Region Of Interest (ROI) visible on Figure 6b;

Preprints (www.preprints.org) | NOT PEER-REVIEWED | Posted: 1 September 2021 doi:10.20944/preprints202109.0019.v1

- Align data coordinate system with specimen material direction, i.e. $11 = MD,\ 22 = CD,\ yy =$ vertical (see Figure 6a);
- Calculate strains from displacements;
- Select subregion and extract the data; all data in the subregion is averaged giving one value of desired quantities per image, namely: $\varepsilon_{11}, \varepsilon_{22}, \varepsilon_{12}, \varepsilon_{yy}$;
- Shear strains are reported as tensor shear strain component ε_{12}, need to be doubled for the engineering component.

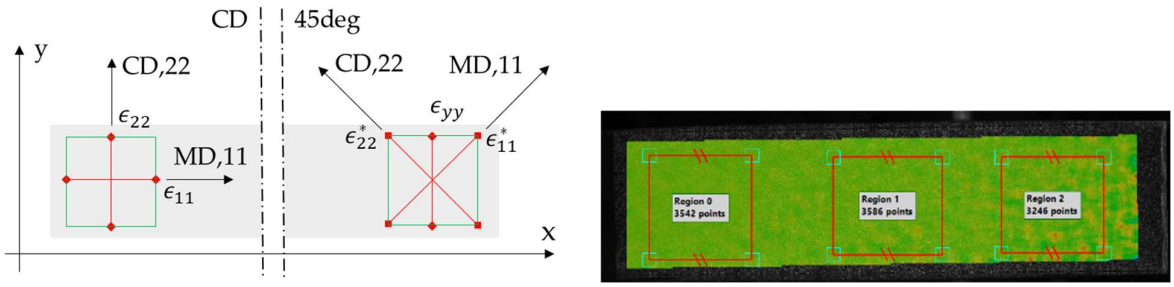

(**a**) (**b**)

Figure 6. Virtual optical gauges (**a**) sample in CD and in 45 deg; (**b**) ROI wisualization.

On the other hand, the video extensometry main procedures, utilized in this study, were as fallow:

- Used speckle pattern compatible with DIC (also the pen marks would work equally well, see [15]);
- Only perpendicular cameras were used (front = Cam1, back = Cam2);
- Length of vertical gauges was 350 pix (see Figure 6 and 7), while length of gauges in 45 deg direction were chosen to be 490 pix, which is $\times 1.4$ of the vertical gauge (see Figure 6a and 7b);
- The three gauges in their respective directions were averaged to produce a single value of strain, i.e. ε_{11}, ε_{22} and ε_{yy} in the 45 deg direction tests or ε_{11} and ε_{22} in CD tests;
- All 'membrane' strain is an average of the front and back strains. Ideally, it should be obtained from the trapezoidal distribution of the paperboard cross-section under combined compression / bending; here it was simply averaged;
- The shear strain can be calculated from the 'strain gauge rosette' (see Figure 7b): $\varepsilon_{12} = \varepsilon_{yy} - 0.5(\varepsilon_{11} + \varepsilon_{22})$.

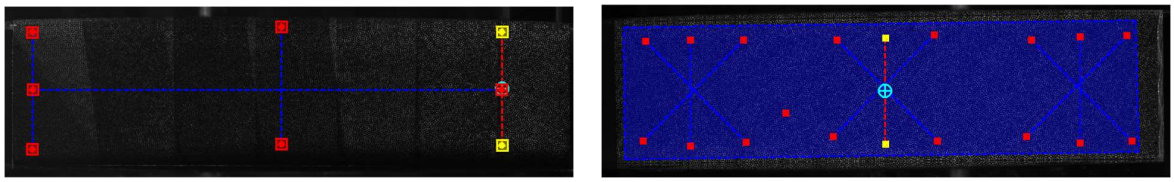

(**a**) (**b**)

Figure 7. Virtual optical gauges (**a**) sample in CD; (**b**) sample in 45 deg.

Using the tests in CD, ε_{yy} (in CD direction) and ε_{xx} (in MD direction) were measured at each image either by averaging large region from DIC (see Figure 6b) or by using virtual extensometers: 3 vertical + 1 horizontal (see Figure 7a). Front and back data were averaged to remove bending artificial data. Similar methodology was used in case of ECT in 45 deg direction. All stiffnesses, e.g., F_{yy} vs ε_{yy} were calculated from the linear portion of the graphs.

Preprints (www.preprints.org) | NOT PEER-REVIEWED | Posted: 1 September 2021 doi:10.20944/preprints202109.0019.v1

*2.4. Proposed method to identify matrix **A***

The identification of matrix **A** is based here on two sets of tests, namely: (a) standard ECT in CD and (b) new ECT in 45 deg direction. The well-known relation between cross-sectional forces and general strains has a form:

$$\begin{bmatrix}\sigma_{11}\\ \sigma_{22}\\ \sigma_{12}\end{bmatrix}=\begin{bmatrix}A_{11} & A_{12} & 0\\ A_{12} & A_{22} & 0\\ 0 & 0 & A_{66}\end{bmatrix}\begin{bmatrix}\varepsilon_{11}\\ \varepsilon_{22}\\ \varepsilon_{12}\end{bmatrix}, \tag{1}$$

where σ_{ij} are the component of sectional force vector, in [N/mm]; A_{ij} are the stiffness components, in [N/mm]; ε_{ij} are the membrane (in-plane) strains.

From the Equation (1) the two set of equation can be extracted, namely in CD test:

$$\begin{aligned}A_{12}\varepsilon_{11}+A_{22}\varepsilon_{22}&=\sigma_{22},\\ A_{11}\varepsilon_{11}+A_{12}\varepsilon_{22}&=0,\end{aligned} \tag{2}$$

and in 45 deg direction test:

$$\begin{aligned}A_{11}\varepsilon_{11}+A_{12}\varepsilon_{22}&=\sigma_{11}^{45}=0.5\sigma^{45},\\ A_{12}\varepsilon_{11}+A_{22}\varepsilon_{22}&=\sigma_{22}^{45}=0.5\sigma^{45}.\end{aligned} \tag{3}$$

By building up a matrix of those equations from the two experiments and solving it in least square sense the component of matrix $A=[A_{11},A_{12},A_{22}]$ can be easily obtained. The component A_{66} can be obtained independently, from the ECT in 45 deg direction.

If one uses stresses instead of sectional forces, the following equations can be derived from the test in CD:

$$\begin{bmatrix}\frac{E_{11}}{1-\nu_{12}\nu_{21}} & \frac{E_{22}\nu_{12}}{1-\nu_{12}\nu_{21}}\\ \frac{E_{11}\nu_{21}}{1-\nu_{12}\nu_{21}} & \frac{E_{22}}{1-\nu_{12}\nu_{21}}\end{bmatrix}\begin{Bmatrix}\varepsilon_{11}\\ \varepsilon_{22}\end{Bmatrix}=\begin{Bmatrix}0\\ \sigma_{22}\end{Bmatrix}, \tag{4}$$

and from the test in 45 deg direction:

$$\begin{bmatrix}\frac{E_{11}}{1-\nu_{12}\nu_{21}} & \frac{E_{22}\nu_{12}}{1-\nu_{12}\nu_{21}}\\ \frac{E_{11}\nu_{21}}{1-\nu_{12}\nu_{21}} & \frac{E_{22}}{1-\nu_{12}\nu_{21}}\end{bmatrix}\begin{Bmatrix}\varepsilon_{11}^{*}\\ \varepsilon_{22}^{*}\end{Bmatrix}=\frac{1}{2}\begin{Bmatrix}\sigma_{45}\\ \sigma_{45}\end{Bmatrix}. \tag{5}$$

From the test in CD only, just two constitutive components can be computed, namely Poisson's ratio:

$$\nu_{21}=-\frac{\varepsilon_{11}}{\varepsilon_{22}}, \tag{6}$$

and elastic modulus in CD:

$$E_{22}=\frac{\sigma_{22}}{\varepsilon_{22}}. \tag{7}$$

On the other hand from both, tests in CD and tests in 45 deg. direction all orthotropic stiffness coefficients can be obtained, namely elastic stiffness in MD:

$$E_{11}=-\frac{\sigma_{22}\sigma_{45}}{\varepsilon_{11}\sigma_{45}-2\varepsilon_{11}^{*}\sigma_{22}}, \tag{8}$$

elastic stiffness in CD:

$$E_{22}=\frac{\sigma_{22}}{\varepsilon_{22}}, \tag{9}$$

Poisson's ratio ν_{12}:

Preprints (www.preprints.org) | NOT PEER-REVIEWED | Posted: 1 September 2021 doi:10.20944/preprints202109.0019.v1

$$\nu_{12} = \frac{\epsilon_{11}\sigma_{45}}{\varepsilon_{11}\sigma_{45} - 2\varepsilon_{11}^{*}\sigma_{22}}, \tag{10}$$

Poisson's ratio ν_{21}:

$$\nu_{21} = 1 - \frac{2\varepsilon_{22}^{*}\sigma_{22}}{\varepsilon_{22}\sigma_{45}}, \tag{11}$$

or using the symmetry principals:

$$\nu_{21} = \nu_{12}\frac{E_{22}}{E_{11}}. \tag{12}$$

The stiffness in 45 deg direction can be computed directly from the test in 45 deg direction:

$$E_{45} = \frac{\sigma_{45}}{\varepsilon_{yy}}, \tag{13}$$

and is used to compute the last missing coefficient, namely in-plane shear stiffness:

$$G_{12} = \left(\frac{2\nu_{12}}{E_{11}} - \frac{1}{E_{11}} - \frac{1}{E_{22}} + \frac{4}{E_{45}}\right). \tag{14}$$

3. Results

3.1. The ECT enhanced with optical measurement techniques

First, the four tests in the CD are presented. Figure 8 shows the differences in the displacements measured by optical techniques (solid line) and taken from the machine crosshead (dashed line).

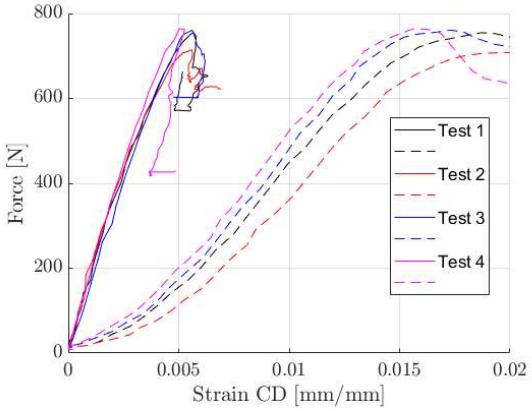

Figure 8. Force-displacement curves. Optical extensometry–solid lines; from machine crosshead–dashed lines.

Table 3. Elastic stiffness index in CD computed from the displacement measurement by the optical extensometry and from machine crosshead, as well as the edgewise compression strength in CD.

Test ID	E - optical (N/mm)	E - crosshead (N/mm)	ECT (N/mm)
1	1,447.45	441.82	-7.548
2	1,380.25	536.82	-7.151
4	1,531.96	450.66	-7.609
5	1,615.12	611.39	-7.640
Mean (N/mm)	1,493.70	510.17	-7.487

Preprints (www.preprints.org) | NOT PEER-REVIEWED | Posted: 1 September 2021 doi:10.20944/preprints202109.0019.v1

Std (N/mm)	102.01	79.93	0.227
Cov (%)	6.829	15.668	-3.038

Table 3 shows the elastic stiffness index, which is computed from the linear part of the curves shown in Figure 8. It is worth noting that the cross-sectional force is normalized by the sample length ($L = 100$ mm) but not by the sample thickness. This approach complies with the specifications of the corrugated board manufacturers and allows the presentation of results regardless of the thickness of the sample.

3.2. DIC vs Extensometry

Then the stereo DIC and the extensometry approach were compared. For this, the selected test in the direction 45 deg. has been carefully analyzed. The DIC data in the zones occupied by extensometers were averaged and compared (see Figure 9 and 10).

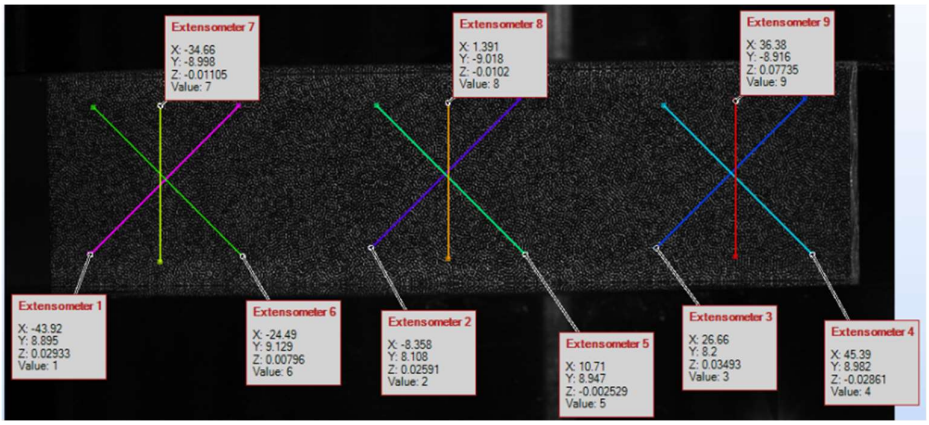

Figure 9. Location of each strain gauge on the sample in the test in a 45-degree direction.

Results presented in Figure 10 are comparable but not identical (in terms of elasticity), mainly due to a certain inhomogeneity in the deformation caused by the crushing of the edges, which obviously affects the extensometers. However, this can be reduced, e.g., by shortening the gauge length, which appears to be a key a priori choice. The question how long should the extensometers be is discussed in the next subsection.

It is known that the error on strain measurements comes from error on measured displacements (here it is constant ~0.01 pixel) and the length of the gauge. Although it seems that the longer the gauge, the better, but the longer the gauge, the greater the risk of taking into account the edge effects of the sample, where (especially in the case of unwaxed samples) the largest local deformations (i.e., crushing and wrinkling) are usually concentrated.

3.3. Length of virtual extensometry

A study on the length of the optical extensometry was run on test no 3 data in CD– full-field data was extracted (i.e., strains and displacements). Virtual extensometers were generated with varied lengths at different horizontal positions and compared against averaged vertical strains from DIC. For example, two points were selected in the center of the sample: one at $Y_1 = +10$ mm with respect to the center of the sample height, the other at $Y_2 = -10$ mm and extensometer strain was calculated from $\varepsilon_{yy} = (v_1 - v_2)/20$.

Preprints (www.preprints.org) | NOT PEER-REVIEWED | Posted: 1 September 2021 doi:10.20944/preprints202109.0019.v1

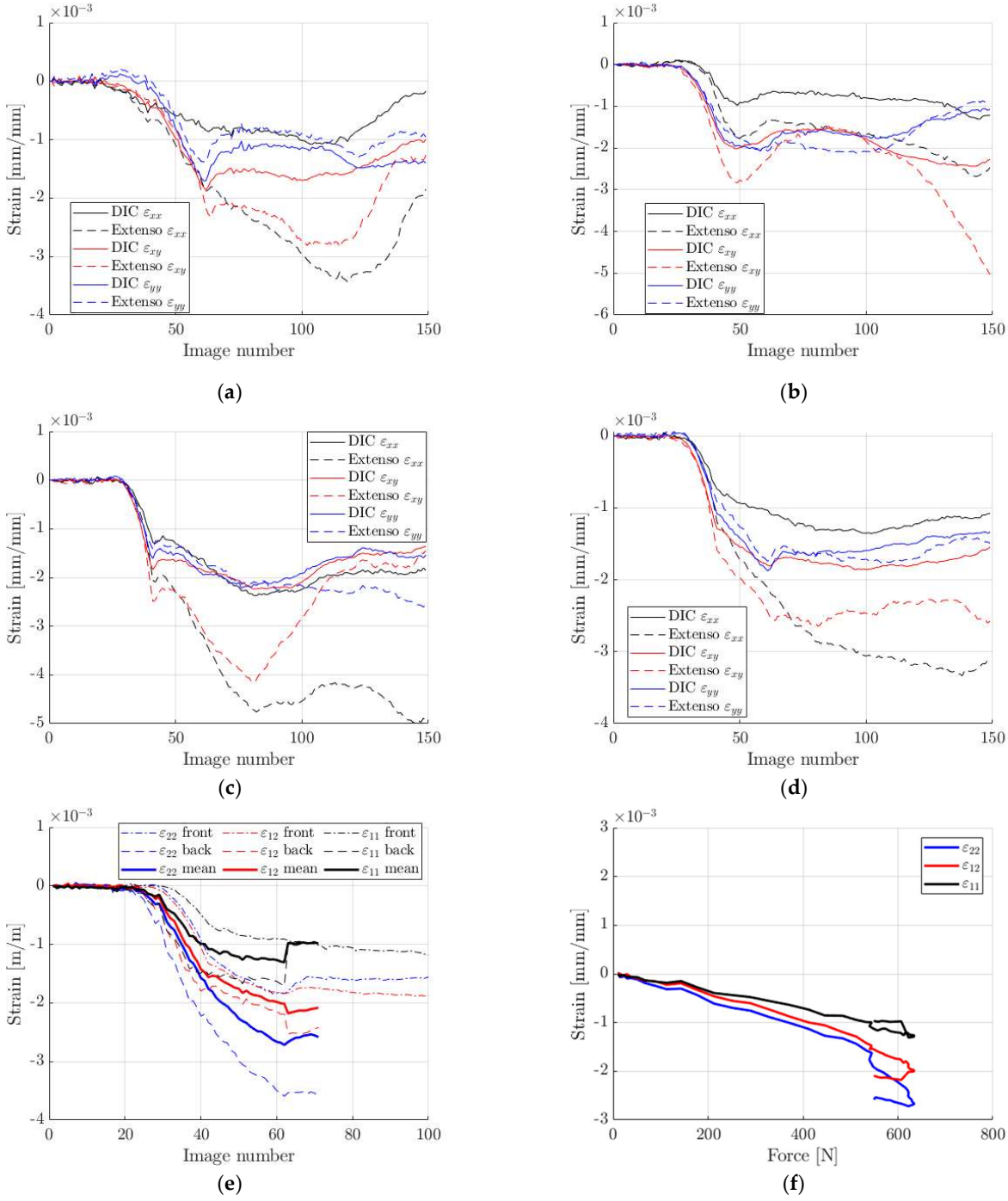

Figure 10. The DIC vs virtual extensometry comparison: (**a**) region 1; (**b**) region 2; (**c**) region 3; (**d**) mean from 3 regions; (**e**) back to front average; (**f**) strains resulting from forces.

Three horizontal positions of the virtual strain gauges were considered: (1) left at 25% of the width; (2) mid at 50% and (3) right at 75% of the sample width. They were also averaged. Figure 11 shows the location of the optical strain gauges. The length of each gauge varies from 4 to 20 mm.

 doi:10.20944/preprints202109.0019.v1

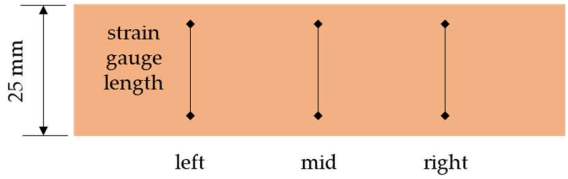

Figure 11. Location of the virtual strain gauges.

Figure 12 shows a comparison of strain calculated while using different lengths of virtual gauges with DIC measurements.

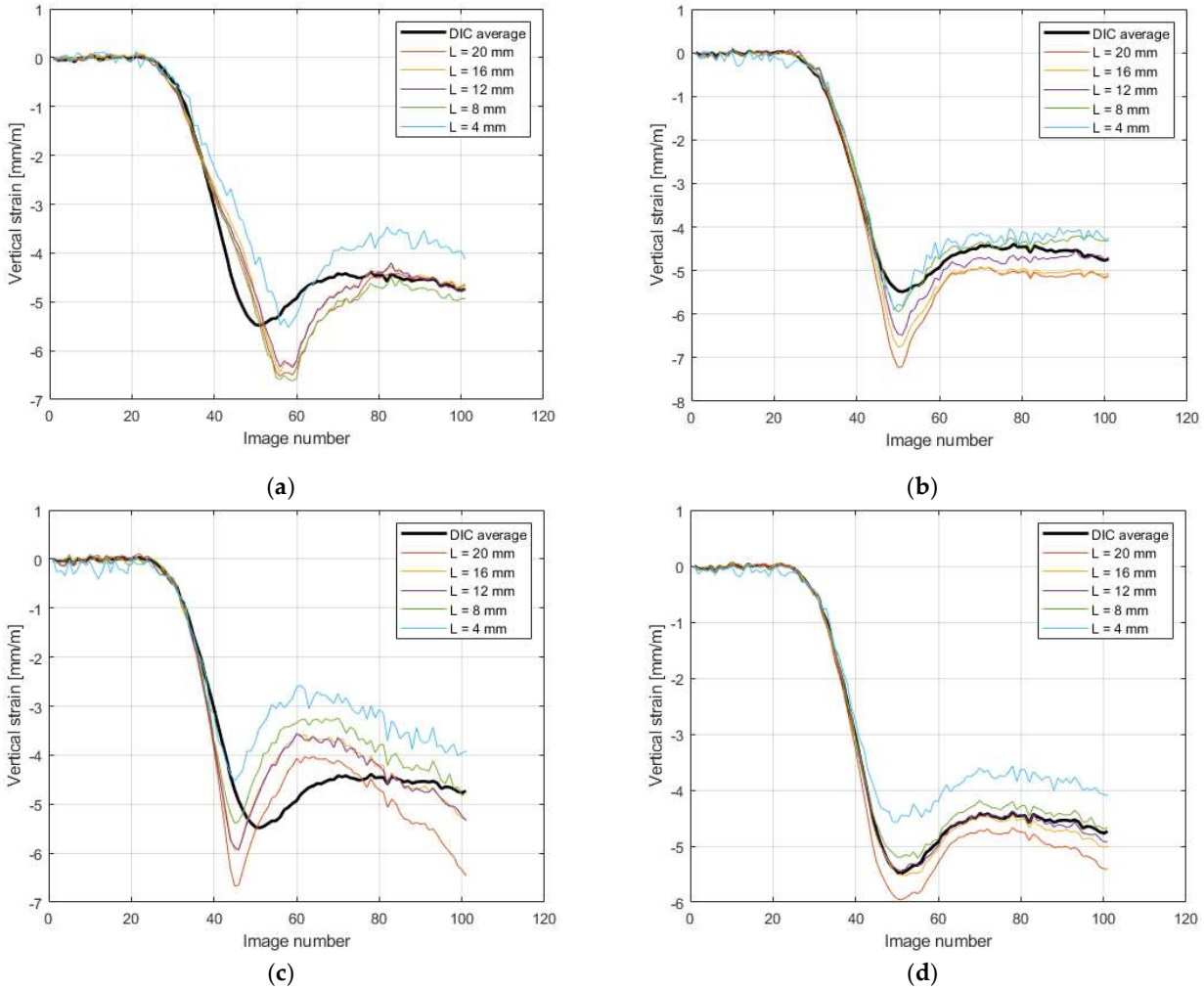

Figure 12. The comparison of strain measured by different length of virtual gauges with DIC measurements. (**a**) left set; (**b**) mid set; (**c**) right set; (**d**) averaged.

The main observation is that for test in 45 deg direction extensometers should be arranged in a rectangular configuration (15 × 15 mm box, with longer gauges on the diagonal) or circular (so as to keep the gauge length of 15 mm).

3.4. Consistency of tests in 45 deg direction.

The last issue was to check data consistency in the new test in 45 deg direction. For all CD tests, the force-strain data was very consistent, but unfortunately not the 45-degree tests. For each recorded level of the force the measured strain components averaged back-

Preprints (www.preprints.org) | NOT PEER-REVIEWED | Posted: 1 September 2021 doi:10.20944/preprints202109.0019.v1

to-front are plotted (see Figure 13). It is visible that the tests can be split into two, more consistent groups (see Figure 14). Group 2 has stiffer response in 11 (MD) direction.

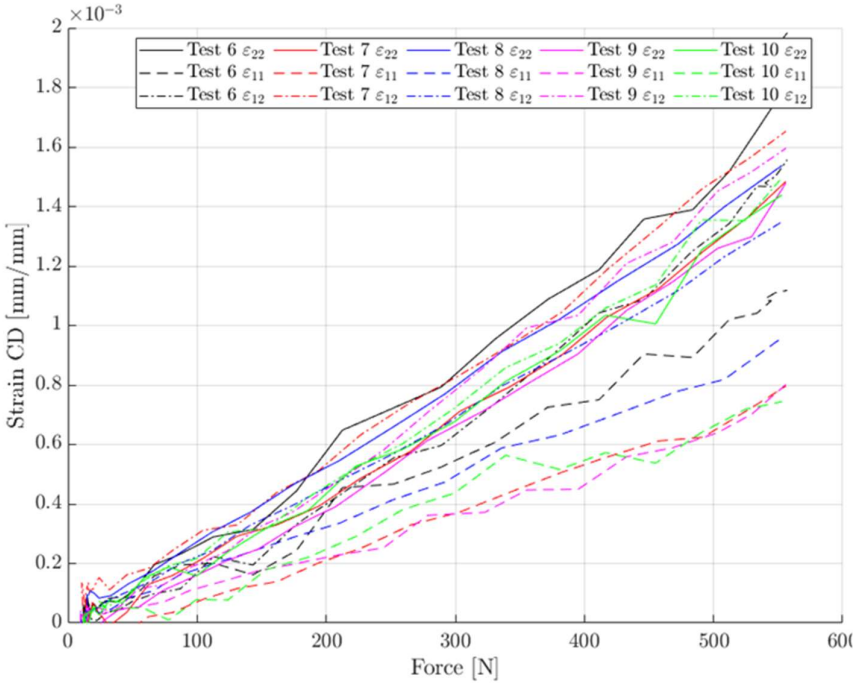

Figure 13. The consistency of data in test 6–10.

The reason for the difference is not fully clear. One of the observation is that group 1 (i.e., test 6 and 8) had high flute oriented towards the stereo DIC setup (front face as depicted in Figure 3c). Local buckling on that face is more pronounced and that could affect measured strains, however, even when using extensometers instead of full DIC, the trend stays the same. Group 1 had (accidently) different orientation of fluting w.r.t. the plate than group 2 (see Figure 3c and 3d).

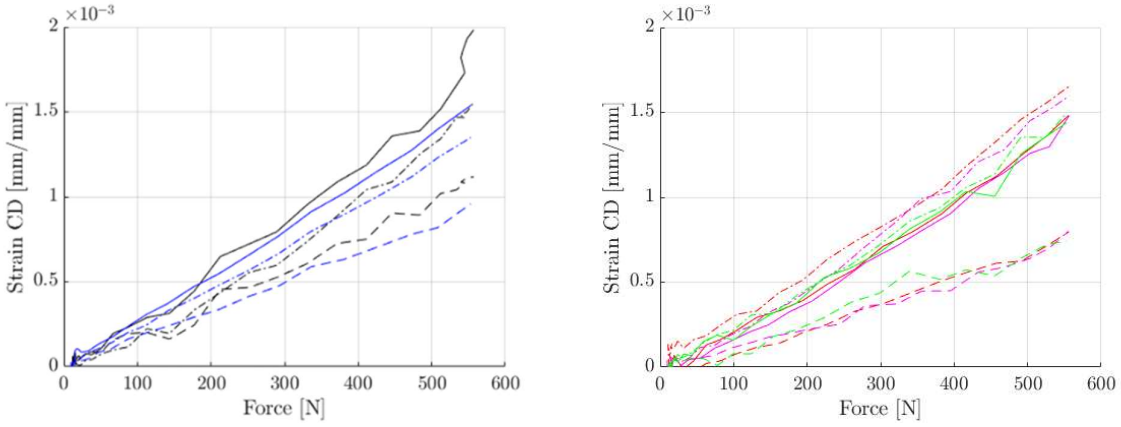

Figure 14. The consistency of data in test 6–10: (**a**) group 1 (test 6 and 8); (**b**) group 2 (test 7, 9 and 10).

3.5. Full matrix A identification

First, by combining tests 2 and 6 and using Equations (2,3) within the least square approximation one can identify the full **A** matrix (see Table 4).

Preprints (www.preprints.org) | NOT PEER-REVIEWED | Posted: 1 September 2021 doi:10.20944/preprints202109.0019.v1

Table 4. The components of **A** matrix.

Parameter:	Test 2 and 6	Group 1	Group 2
A_{11} (N/mm)	2581	2583.0	3554.0
A_{12} (N/mm)	158	103.5	158.1
A_{22} (N/mm)	1674 (1500 [1])	1765.0	1792.0
A_{66} (N/mm)	1078	1061.0	946.0

[1] Results obtained directly from test 2 in CD using Equation (7) or (9).

Poisson's ratio computed directly from CD test (see Equation (6)) turned out to be ~0.07 which is much close to the value cited here: $A_{12}/A_{22} = 0.09$. In all cases force was normalized by the specimen width (100 mm). In the investigation the test no 1 was removed from the data pool due to an artefact point.

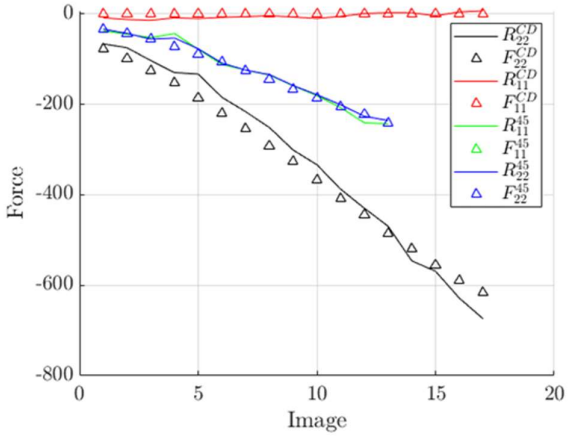

Figure 15. Curves reconstructed from identified **A** matrix vs measured force.

Finally, the same procedure as above was used, but with the two separate groups discussed in previous subsection and shown in Figure 14. In total 178 (grp 1) and 204 (grp 2) points were used here to calculate in-plane stiffnesses (A_{11}, A_{12}, A_{22}). This separation made it possible to study the effect of positioning unsymmetric samples on the ECT apparatus.

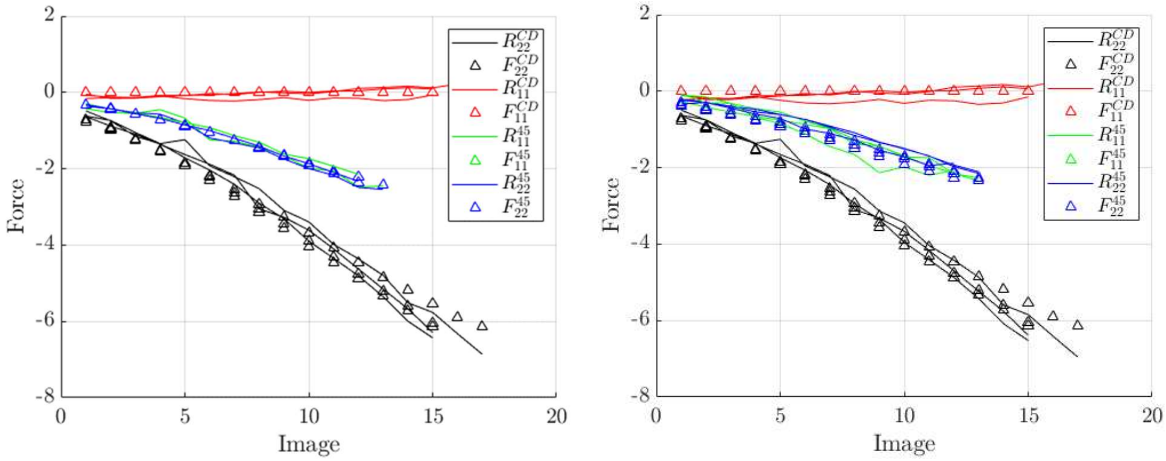

(**a**) (**b**)

Figure 16. Curves reconstructed from identified **A** matrix vs measured force: (**a**) using tests in group 1; (**b**) using test in group 2.

 doi:10.20944/preprints202109.0019.v1

Reconstructed elastic forces are shown in Figure 15 and 16, from the identified parameters–multiple lines represent multiple tests. Data show good model fitting.

4. Discussion

The previous section presents the results of the research, showing, among others, typical ECT results enriched with Digital Image Correlation and / or optical, virtual extensometry techniques. The results summarized in Table 3 clearly show that the use of the displacements obtained from the machine crosshead introduces an error in the estimation of the stiffness index, underestimating this value almost 3 times. The same observation can also be found in the recent work of Garbowski et al. [15]. The compressive strength given in Table 3 (shown in column 4) is consistent with the value provided by the manufacturer of the corrugated board, namely 7.6 N/mm $\pm$10%.

The comparison of strains obtained from DIC and using virtual extensometers is presented in Figure 10. The results are comparable but not identical. Best fit can be observed for the vertical strain ε_{yy}. Based on the observations regarding the length of the optical extensometer and its influence on the accuracy of the results, 15 mm segments were used for further analyzes. This can be observed in Figure 12, where the calculated strains were compared while using DIC and extensometers of different lengths. The main conclusion is that when applying longer gauges, the results are more stable. However, if the optical extensometer is too long (i.e., longer than 15 mm) or to short (i.e., shorter than 8 mm), the differences can be as high as 15%.

The use of extensometers with a length of ~20 mm causes false results due to the proximity of the measuring tip to the crushed edge of the sample (which is 25 mm high). On the other hand, the use of short gauges of ~5mm is affected by larger noise and causes the measurements to have an error due to buckling from the plane of the sample (see Figure 17b). The moment when the sample buckles is shown in Figure 12d–image number 38 (for a strain gauge 4 mm long). The influence of buckling (which manifests in the form of out-of-plane deformation) on the measurement of in-plane deformations can be easily eliminated by using the stereo DIC procedure. However, if the optical extensometry is to be used, a fairly large area where the results obtained with the extensometer match those obtained with the DIC should be in the range of 8-16 mm.

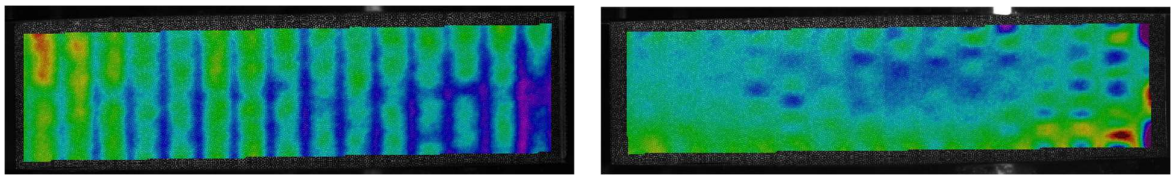

(**a**) (**b**)

Figure 17. The ECT sample during the test in CD: (a) sample during the test in CD–no buckling; (**b**) sample during the test in CD–buckling.

Table 4 shows the identified components of matrix **A**. The second column shows the results obtained during tests 2 and 6, while columns 3 and 4 show the results obtained while using two different test groups. The groups included samples with a higher flute from the front (on the side of the DIC stereo set) and samples with a lower flute from the front. It is evident that the results for group 2, especially in the case of A_{11} and A_{12}, differ significantly from the results obtained in the first procedure and while using group 1. This is due to the asymmetric cross-section of the sample and the different level of buckling on the sample side with higher flute. Out-of-plane deformation related to buckling distorts the measurement and therefore introduces noise that distorts the results. Other components of **A** matrix do not differ more than 10% when using different measurement techniques, which is very promising.

 doi:10.20944/preprints202109.0019.v1

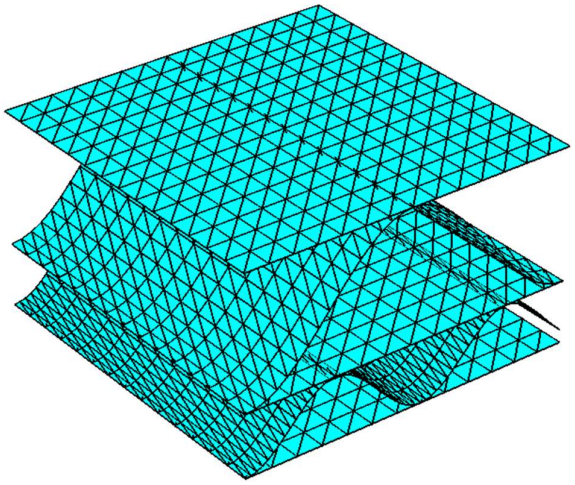

Figure 18. Visualization of the finite element model of corrugated board BE-650.

In order to validate the results presented in Table 4 the numerical homogenization procedure (for details see recent works by Garbowski & Gajewski [9] or Garbowski et al. [10]) of the cross-section of the corrugated board BE-650 (see Figure 18) was used. The numerical homogenization techniques used the geometrical and constitutive parameters presented in Table 1 and 2. The following results were obtained using the homogenization technique: $A_{11} = 2620$ N/mm, $A_{12} = 185$ N/mm, $A_{22} = 1812$ N/mm, $A_{66} = 906$ N/mm. The results are in good agreement, which proves that the use of optical techniques in conjunction with the new setup of the ECT (samples cut at an angle of 45 degrees wrt direction of corrugation) can be effective in determining the stiffness of corrugated cardboard.

5. Conclusions

The main conclusion is that stereo DIC and / or optical extensometry techniques can be used to evaluate stiffness in a standard edge crush test. In order to determine all the stiffness coefficients, it is necessary to use an additional, new test specimen cut at an angle of 45 degrees to the direction of the corrugation. By applying results from two samples simultaneously and using a least squares minimization approach, all stiffness components can be easily identified. The only concern is the proper surface selection in unsymmetrical corrugated cardboard samples for stereo DIC measurement, especially in 45-degree tests. However, this is easily remedied by using a larger sample set and averaging the results.

Author Contributions: Conceptualization, T.G.; methodology, T.G.; software, T.G. and A.M.; validation, A.M., A.K.-P. and T.G.; formal analysis, A.M. and T.G.; investigation, A.M., A.K.-P. and T.G.; resources, A.M.; data curation, A.M.; writing—original draft preparation, A.K.-P. and T.G.; writing—review and editing, A.K.-P., T.G. and A.M.; visualization, A.M. and T.G.; supervision, T.G.; project administration, T.G.; funding acquisition, A.K.-P. and T.G. All authors have read and agreed to the published version of the manuscript.

Funding: The APC was funded by the Ministry of Science and Higher Education, Poland, the statutory funding at Poznan University of Life Sciences, grant number 506.569.05.00 and the statutory funding at Poznan University of Technology, grant number 0411/SBAD/0004.

Institutional Review Board Statement: Not applicable.

Informed Consent Statement: Not applicable.

Acknowledgments: Special thanks to the FEMat Sp. z o. o. company (Poznań, Poland) (www.fematsystems.pl— accessed on 21 July 2021) for providing the laboratory equipment and commercial software.

Conflicts of Interest: The authors declare no conflict of interest.

References

1. Kellicutt, K.; Landt, E. Development of design data for corrugated fibreboard shipping containers. *Tappi J.* **1952**, *35*, 398–402.
2. Maltenfort, G. Compression strength of corrugated containers. *Fibre Contain*. **1956**, *41*, 106–121.
3. McKee, R.C.; Gander, J.W.; Wachuta, J.R. Compression strength formula for corrugated boxes. *Paperboard Packag*. **1963**, *48*, 149–159.
4. Magnucka-Blandzi, E.; Magnucki, K.; Wittenbeck, L. Mathematical modeling of shearing effect for sandwich beams with sinusoidal corrugated cores. *Appl. Math. Model.* **2015**, *39*, 1796–2808.
5. Magnucka-Blandzi, E.; Magnucki, K. Transverse shear modulus of elasticity for thin-walled corrugated cores of sandwich beams. Theoretical study. *J. Theor. Appl. Mech.* **2014**, *52*, 971–980.
6. Nordstrand, T.M.; Carlsson, L.A. Evaluation of transverse shear stiffness of structural core sandwich plates. *Comp. Struct*. **1997**, *37*, 145–153.
7. Garbowski, T.; Gajewski, T.; Grabski, J.K. Role of transverse shear modulus in the performance of corrugated materials. *Materials* **2020**, *13*, 3791.
8. Garbowski, T.; Gajewski, T.; Grabski, J.K. Torsional and transversal stiffness of orthotropic sandwich panels. *Materials* **2020**, *13*, 5016.
9. Garbowski, T.; Gajewski, T. Determination of transverse shear stiffness of sandwich panels with a corrugated core by numerical homogenization. *Materials* **2021**, *14*, 1976.
10. Garbowski, T.; Knitter-Piątkowska, A.; Mrówczyński,D. Numerical homogenization of multi-layered corrugated cardboard with creasing or perforation. *Materials* **2021**, *14*, 3786.
11. Domaneschi, M.; Perego, U.; Borgqvist, E.; Borsari, R. An industry-oriented strategy for the finite element simulation of paperboard creasing and folding. *Packag. Tech. Sci*. **2017**, *30*, 269–294.
12. Garbowski, T.; Gajewski, T.; Grabski, J.K. The role of buckling in the estimation of compressive strength of corrugated cardboard boxes. Materials 2020, 13, 4578.
13. Garbowski, T.; Gajewski, T.; Grabski, J.K. Estimation of the compressive strength of corrugated cardboard boxes with various openings. *Energies* **2021**, *14*, 155.
14. Garbowski, T.; Gajewski, T.; Grabski, J.K. Estimation of the compressive strength of corrugated cardboard boxes with various perforations. *Energies* **2021**, *14*, 1095.
15. Garbowski, T.; Grabski, J.K.; Marek, A. Full-field measurements in the edge crush test of a corrugated board—analytical and numerical predictive models. *Materials* **2021**, *14*, 2840.
16. Gajewski, T.; Garbowski, T.; Staszak, N.; Kuca, M. Crushing of double-walled corrugated board and its influence on the load capacity of various boxes. *Energies* **2021**, *14*, 4321.
17. Kmita-Fudalej, G.; Szewczyk, W.; Kołakowski, Z. Calculation of honeycomb paperboard resistance to edge crush test. *Materials* **2020**, *13*, 1706.
18. Park, J.; Park, M; Choi, D.S.; Jung, H.M.; Hwang, S.W. Finite element-based simulation for edgewise compression behavior of corrugated paperboard for packaging of agricultural products. *Appl. Sci*. **2020**, *10*, 6716.
19. Wong, J.E.; Mustapha, K.B.; Shimizu, Y.; Kamiya, A.; Arumugasamy, S.K. Development of surrogate predictive models for the nonlinear elasto-plastic response of medium density fiberboard-based sandwich structures. *Int. J. Lightweight Mater. Manuf.* **2021**, *4*, 302–314.
20. Marek, A.; Garbowski, T. Homogenization of sandwich panels. *Comput. Assist. Methods Eng. Sci.* **2015**, *22*, 39–50.
21. Hohe, J. A direct homogenization approach for determination of the stiffness matrix for microheterogeneous plates with application to sandwich panels. *Compos. Part B* **2003**, *34*, 615–626.
22. FEMat Systems. Available online: http://fematsystems.pl/home_en (accessed on 25 April 2021).
23. TAPPI T 839 om-12. *Edge Compression Test for Strength of Corrugated Fiberboard Using the Clamp Method (Short Column Test)*; TAPPI: Peachtree Corners, GA, USA, 2009.
24. TAPPI T 838 cm-12. *Edge Crush Test Using Neckdown*; TAPPI: Peachtree Corners, GA, USA, 2009.
25. FEFCO NO.8. *Edgewise Crush Resistance of Corrugated Fiberboard*; FEFCO: Brussel, Belgium, 1997.
26. ISO 3037:2013. *Corrugated Fibreboard—Determination of Edgewise Crush Resistance (Unwaxed Edge Method)*; ISO: Geneva, Switzerland, 2013.
27. TAPPI T 811 om-11. Edgewise Compressive Strength of Corrugated Fibreboard (Short Column Test); TAPPI: Peachtree Corners, GA, USA, 2009.
28. ISO 13821:2002. Corrugated Fibreboard—Determination of Edgewise Crush Resistance—Waxed Edge Method; ISO: Geneva, Switzerland, 2002.
29. Hägglund, R.; Åslund, P.E.; Carlsson, L.A.; Isaksson, P. Measuring thickness changes of edgewise compression loaded corrugated board panels using digital image correlation. *J. Sandwich Struct. Mater*. **2010**, *14*, 75–94.
30. Viguié, J.; Dumont, P.J.J.; Vacher, P.; Orgéas, L.; Desloges, I.; Mauret, E. Analysis of the strain and stress field of cardboard box during compression by 3D Digital Image Correlation. *Appl. Mech. Mater*. **2010**, *24–25*, 103–108.
31. Viguié, J.; Dumont, P.J.J.; Orgéas, L.; Vacher, P.; Desloges, I.; Mauret, E. Surface stress and strain fields on compressed panels of corrugated board boxes. An experimental analysis by using Digital Image Stereocorrelation. *Comp. Struct*. **2011**, *93*, 2861–2873.

32. Viguié, J.; Dumont, P.J.J. Analytical post-buckling model of corrugated board panels using digital image correlation measurements. *Comp. Struct*. **2013**, *101*, 243–254.
33. Borgqvist, E.; Lindström, T.; Tryding, J.; Wallin, M.; Ristinmaa, M. Distortional hardening plasticity model for paperboard. *Int. J. Solids Struct*. **2014**, *51*, 2411–2423.
34. Cocchetti, G.; Mahini, M.R.; Maier, G. Mechanical characterization of foils with compression in their planes. *Mech. Adv. Mater. Struct*. **2014**, *21*, 853–870.
35. Garbowski, T.; Maier, G.; Novati, G. On calibration of orthotropic elastic-plastic constitutive models for paper foils by biaxial tests and inverse analyses. *Struct. Multidisc. Optim.* **2012**, *46*, 111–128.
36. Considine, J.M.; Pierron, F.; Turner, K.T.; Vahey, D.W. General anisotropy identification of paperboard with virtual fields method. *Exp. Mech.* **2014**, *54*, 1395–1410.
37. Åslund, P.E.; Hägglund, R.; Carlsson, L.A.; Isaksson, P. An analysis of strain localization and formation of face wrinkles in edgewise loaded corrugated sandwich panels using a continuum damage model. *Int. J. Solids Struct*. **2015**, *56–57*, 248–257.
38. Zappa, E.; Liu, R.; Bolzon, G.; Shahmardani, M. High resolution non-contact measurement techniques for three-dimensional deformation processes of paperboard laminates. *Mater. Today Proc*. **2017**, *4*, 5872–5876.
39. Fadiji, T.; Coetzee, C.J.; Opara, U.L. Evaluating the displacement field of paperboard packages subjected to compression loading using digital image correlation (DIC). *Food Bioprod. Process*. **2020**, *123*, 60–71.